Available online at www.sciencedirect.com
ScienceDirect
Trans. Nonferrous Met. Soc. China 27(2017) 986−997
Transactions of Nonferrous Metals Society of China
www.tnmsc.cn

Optimization of friction and wear behaviour of Al−Si_3N_4 nano composite and Al−Gr−Si_3N_4 hybrid composite under dry sliding conditions

R. AMBIGAI, S. PRABHU

Department of Mechanical Engineering, SRM University, Chennai 603203, India

Received 25 April 2016; accepted 30 September 2016

Abstract: The tribological behaviour of gravity die stir cast LM6 alloy with graphite (Gr) and silicon nitride nanoparticles was investigated. Al−Gr−Si_3N_4 hybrid composite, Al−Si_3N_4 nanocomposite and Al−Gr nanocomposites were separately fabricated to investigate their frictional and wear characteristics under dry sliding conditions. EDS was used to ensure the uniform presence of nano Si_3N_4 and graphite in the cast. L9 orthogonal array method was chosen to conduct the experiments to study the effect of different applied loads (20, 30 and 40 N) and sliding distances (1, 2 and 3 km). The results showed that the respective wear rate and coefficient of friction (COF) decreased by 25% and 15% for hybrid composite when compared with those of Al−Si_3N_4 nanocomposite whereas the wear rate and COF of Al−Gr was found to be very minimal. The micro Vickers hardness of the hybrid composite was 14% more than that of the simple nanocomposite and there was not much notable variation for Al−Gr and Al−Si_3N_4 nanocomposite materials. Scanning electron microscope was used to analyze the worn surface and subsurface, from which it was noted that the predominant wear mechanisms observed were abrasive for nanocomposite and both abrasive and adhesive mechanism for hybrid composite. Analysis of variance (ANOVA) and *F*-test were used to check the validity model and to determine the significant parameters affecting the wear rates.

Key words: abrasive wear; Si_3N_4; graphite; hybrid composite; load; sliding distance; ANOVA

1 Introduction

Composite consists of one or more discontinuous phases properly embedded in a continuous phase. The discontinuous phase is usually harder and stronger than the continuous phase and is called the reinforcement or the reinforcing material, whereas the continuous phase is termed as the matrix. Properties of composites are strongly dependent on the properties of their constituent materials, their distribution in the matrix and the interaction among them. Metal matrix composites (MMCs) generally offer higher specific strength, higher stiffness and better wear resistance resulting in increasing use in the aerospace, automotive and biomedical industries. Popular reinforcement materials for these composites are silicon carbide, silicon nitride, boron carbide, alumina particles, with aluminium, titanium and magnesium being the most common matrix materials. The aluminium-based composite materials having ceramic reinforcements are found to reveal improved quality, specific strength, higher temperature properties, higher wear resistance and lower thermal expansion coefficient with better corrosion resistance in comparison with their base alloy matrixes. At present, more research consideration is being directed towards identifying hybrid composites having more than one reinforcing component. KAUSHIK and RAO [1] developed and investigated the two-body abrasive wear behavior of stir cast Al6082−SiC−Gr (Al−SiC−Gr) hybrid composites and compared them with their matrix alloy and SiC reinforced composites. The wear results indicated that the hybrid composites yielded better wear resistance compared with the matrix alloy and SiC-reinforced composites. SAEED et al [2] produced Al/WO_3/SiC hybrid nanocomposite using Al1050 sheets and WO_3 and SiC nanoparticles through accumulative roll bonding (ARB) process. Uniaxial tensile test and hardness measurement were carried out on ARBed specimens. The results revealed that by increasing the number of ARB cycles, a better distribution of WO_3 and SiC nanoparticles was obtained in the Al matrix. So, after

Corresponding author: S. PRABHU; E-mail: prabhume@yahoo.co.in
DOI: 10.1016/S1003-6326(17)60116-X

the 9th cycle, the hybrid nanocomposite showed an excellent distribution of the nanoparticles with strong bonding between the nanoparticles and the aluminum matrix.

KENNETH et al [3] investigated the corrosion and wear behaviour of Al−Mg−Si alloy hybrid composites with the use of rice husk ash (RHA) and silicon carbide (SiC) particulates as reinforcements. The corrosion and wear mechanisms were established with the aid of scanning electron microscopy. The results showed that the effect of RHA/SiC mass ratio on the corrosion behavior of the composites in 3.5% NaCl solution was not consistent for different mass fractions of reinforcement (5%, 7.5% and 10%) used in developing the Al−Mg−Si-based composites. It was evident that for most cases, the use of hybrid reinforcement of RHA and SiC resulted in improved corrosion resistance of the composites in 3.5% NaCl solution. SARADA et al [4] produced aluminium hybrid metal matrix composite (LM 25-activated carbon-mica) by stir casting method and compared the properties with conventional composites. POZDNIAKOV et al [5] discussed the reinforcement of B_4C particles by stir casting and a good interface reaction between the matrix and the B_4C reinforcements was observed by the formation of Al_3BC and AlB_2 phases at the matrix/ B_4C interface. BALAJI et al [6] studied the effect of various properties like tensile strength and hardness of Al7075 and Al6061 after reinforcing with SiC particles by stir casting; they observed that there was an increase in strength and hardness by 10% compared with Al6061.

HAMID et al [7] fabricated Al6061/nano Al_2O_3 composites by stir casting process through injection of Al_2O_3 particles into the molten Al alloy by argon gas along with stirring using a mechanical stirrer. The nanocomposites were then extruded at 550 °C. It was observed that with increasing amount of Al_2O_3 nanoparticles, yield strength and tensile strength increased but elongation decreased. YIN et al [8] studied the friction and wear behavior of Al_2O_3/TiC micro-nano-composite ceramic sliding against metals (stainless steel, chrome steel) and hard materials (cemented carbide, Si_3N_4). When sliding against stainless steel, the friction coefficient was the smallest but the wear rate was the largest. The smallest friction coefficient was due to the metal adhesion layer that was formed by the chemical reaction between iron oxides and Al_2O_3. The rough wear surface and lack of metal adhesion layer were responsible for the high friction coefficient in the case of sliding against hard materials. The primary wear mechanism of Al_2O_3/TiC composite ceramic sliding against stainless steel was adhesion, while abrasion and chipping were observed to be the main wear mechanisms in the case of sliding against chrome, cemented carbide and Si_3N_4. PARDEEP et al [9] studied the fabrication of silicon nitride reinforced composites for various mass fractions of silicon nitride particles by conventional stir casting route. The microstructure and mechanical properties of the fabricated composites were investigated. The results showed that mechanical properties such as ultimate tensile strength and hardness improved at the cost of reduction in ductility with increase in mass fraction of silicon nitride. The density and porosity of the composites also showed an increasing trend with increase in volume fraction of Si_3N_4 particles. XIU et al [10] observed that the bending strength of Si_3N_4/Al composites decreased with an increase in Si_3N_4 volume fraction, and could be greatly improved by T6 treatment. Elastic modulus of composites increased linearly with Si_3N_4 volume fraction.

XIU et al [10] fabricated Si_3N_4 particles reinforced aluminium matrix composites (Si_3N_4/Al) with different particle volume fractions (45%, 50% and 55%) by pressure infiltration method. The effects of Si_3N_4 volume fraction and T6 treatment on microstructure and mechanical properties of Si_3N_4/Al composite were investigated. The results showed that Si_3N_4/Al composites were well infiltrated with good particle dispersion and no apparent porosity or significant casting defects were observed. High density of dislocations in Al matrix around Si_3N_4 particles was observed. The bending strength of Si_3N_4/Al composites decreased with an increase in Si_3N_4 volume fraction, and could be greatly improved by T6 treatment. Elastic modulus of composites increased linearly with Si_3N_4 volume fraction. MATHAN et al [11] proposed that Al2618 alloy was taken as the matrix material along with reinforcement particles such as silicon nitride (Si_3N_4), aluminium nitride (AlN) and zirconium boride (ZrB_2). It was well mixed with Al2618 alloy in various mass fractions (0, 2%, 4%, 6% and 8%) by stir casting method. The mechanical properties like hardness, tensile strength, compressive strength for Al2618 composites were increased along with increasing the mass fraction of reinforcement. A new attempt was made to optimize the parameters to obtain minimum value in material removal rate, tool wear rate and depth through electrical discharge machining process (EDM) at elevated temperatures.

WANG et al [12] prepared a new Ni−P−Si_3N_4 nanowire composite coating on AZ31 Mg substrate through electroless deposition technique. The effects of Si_3N_4 nanowire concentration in the plating bath on the surface morphology, hardness and wear behavior of the composite coatings were investigated. The results showed that when the concentration of Si_3N_4 nanowire was 1.5 g/L, the morphology of composite coating appeared as fine nodular structure. HUANG et al [13]

mentioned that to determine the effective content of Si_3N_4 on microstructures and antioxidant properties of $MoSi_2/Si_3N_4$ composite coatings on Mo substrate, the $MoSi_2$−x%Si_3N_4/Mo diffusion couples were fabricated by spark plasma sintering and annealed at 1300 °C for various periods of time up to 168 h. The interfacial diffusion between $MoSi_2$−Si_3N_4 phase and Mo substrate was examined. TOMASZ et al [14] studied the influence of graphene (1% addition of graphene, mass fraction) and varied the sintering temperature in order to achieve composites with high mechanical properties and physical properties of Si_3N_4 and Si_3N_4-graphene composites. The highest relative density (99.31% and 99.32%) and fracture toughness (K_{IC}=6.0 MPa·m$^{0.5}$) were measured for samples sintered at 1650 and 1700 °C respectively and there was no increase of fracture toughness between pure silicon nitride sinter and composite with 1% of graphene. JAN et al [15] studied the mechanical and tribological properties of nanocomposites for both high and room temperatures of silicon nitride matrix with addition of 1% and 3% of multilayered graphene (MLG) platelets. Addition of MLG did not lower the coefficient of friction. Graphene platelets were integrated into the matrix very strongly and they did not participate in lubricating processes. JAN et al [15] observed that the best performance was observed at room temperature with 3% of graphene, which had the highest wear resistance. Wear resistance at high temperatures significantly decreased. BARADESWARAN et al [16] proposed that aluminium alloys 6061 and 7075 were reinforced with 10% of boron carbide (B_4C) and 5% of graphite through liquid casting technique. AA7075/B_4C/graphite hybrid composite exhibited higher wear resistance property compared with base alloys and AA6061 hybrid composite.

From the literature survey, it is found that much work has not been carried out to investigate the tribological behavior of Al−Si_3N_4 nanocomposites as brake pad material. Similarly, even less work has been reported on tribological behavior of aluminium-based graphite and Si_3N_4 hybrid composite. Hence, it was decided to conduct an in-depth study on friction and wear behavior of Al−Si_3N_4 nanocomposite and Al−Gr−Si_3N_4 hybrid composite under dry sliding conditions, and to optimize the parameters.

2 Experimental

Al−Si alloy was used as matrix alloy and Si_3N_4 particulates with a nominal size of 500−600 nm and Gr powder were used as reinforcement phases. The composition of the Al−Si alloy chosen for the investigation was: 10% Si, 0.10 % Mg, 0.10% Cu, 0.50% Mn, 0.60% Fe, 0.20% Ti and rest Al. The mechanical properties of Al−Si, graphite and nano Si_3N_4 are shown in Tables 1−3. The composite required for the investigation was fabricated by gravity die stir-casting technique. The final composites were cast to the size of 25 mm.

Table 1 Mechanical properties of Al−Si alloy

Property	Value
Density/(g·cm^{-3})	2.65
Melting point/°C	660
Brinell hardness	50−55
Elastic modulus/GPa	71

Table 2 Mechanical properties of graphite

Property	Value
Density/(g·cm^{-3})	2.26
Melting point/°C	3500
Elastic modulus/GPa	11

Table 3 Mechanical properties of nano Si_3N_4

Property	Value
Density/(g·cm^{-3})	3.23
Melting point/°C	1900
Brinell hardness	2200
Elastic modulus/GPa	28.0−46.0
Bending strength/MPa	147
Compressive strength/MPa	490

2.1 Processing route

Gravity die stir casting setup was used to melt the aluminum alloy. The furnace was switched on after setting the graphite crucible with required quantity of aluminum, with needed flux added to it. Sufficient time was allowed for the aluminum to melt and the furnace was maintained at 850 °C for 0.5 h. 3.33% (mass fraction) of nano Si_3N_4 was taken in another graphite crucible and preheated for 1 h before mixing, which ensured uniform distribution of nano Si_3N_4 particle in alloy. The heated nano Si_3N_4 was then added slowly through a funnel into the melt. The stirrer of the furnace was kept switched on at this time so as to ensure uniform distribution of nano Si_3N_4 in the molten matrix. The gravity die stir casting setup is shown in Fig. 1(a). The molten final mixture was then poured into the die by gravity and the die was then allowed to cool to reach room temperature. The cast Al−Si_3N_4 nanocomposite is shown in Fig. 1(b). A similar procedure was used to fabricate the other Al−Gr composite and Al−Gr−Si_3N_4 hybrid composite using 3.33% of Gr powder and Si_3N_4 heated additives in a graphite crucible added to the melt to make hybrid composite.

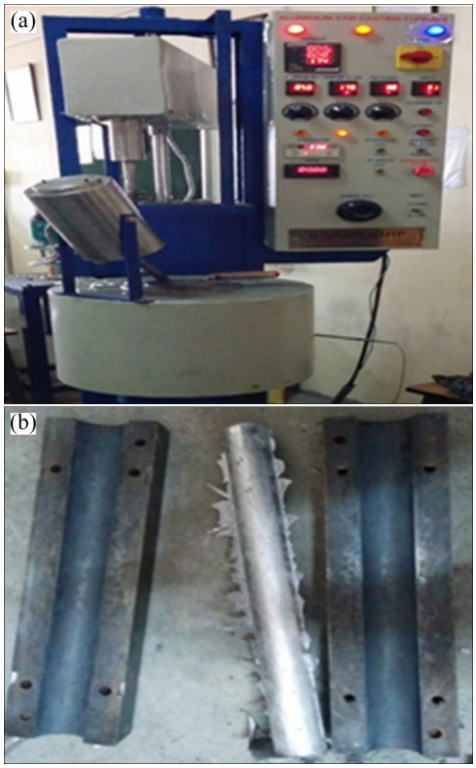

Fig. 1 Stir casting setup (a) and cast sample (b)

2.2 Tribology tests

In order to characterize the tribological properties of the composite, the experiments were performed using a computer controlled pin-on-disc tribometer (Ducom, Bangalore, India) as shown in Fig. 2 under ambient conditions of temperature (room temperature) and humidity. Dry sliding test was carried out as per ASTM G99 test standards. EN31 steel disc with the hardness of HRC 60 and ground to surface finish with roughness (R_a) of 1.6 μm was mounted and firmly secured perpendicularly to the axis of rotation. The wear test specimens were machined into pins of size 10 mm in diameter, 25 mm in length using EDM from the cast composite, as shown in Fig. 3. The ends of the specimens were polished with abrasive paper of grade 1/0 followed by grade 4/0. The external surfaces of the pins were cleaned with acetone and weighed before and after the test to an accuracy of ±0.0001 g to determine the amount of wear. The pin specimen was inserted in its holder and adjusted so that the specimen was perpendicular to the disc surface when in contact. Appropriate load cells from 20 to 40 N were added to the system lever to develop the selected force pressing the pin against the disc. The counter balance weights were adjusted, so that the load was acting over its entire cross-section. The data on the electrical display unit showed the extent of load acting tangentially on the disc and the depth of wear, which increased with the application of load. Initially, the displacement sensor and the tangential force sensor were adjusted and set to zero at start without load; later, the tangential force and the pin displacement were measured. This tangential component data was used for calculating the friction component. The signals from sensors after processing in PID controller were transmitted to the PC and were displayed on the software screen. The software used for acquiring these data was WINDUCOM 2008. Table 4 summarizes the range of wear test parameters.

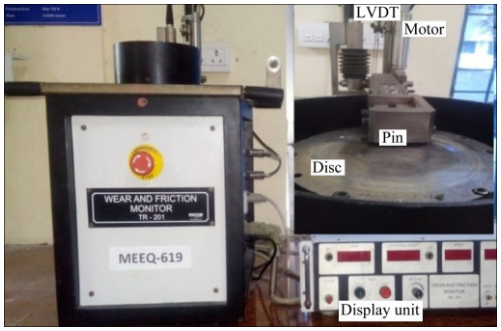

Fig. 2 Wear testing equipment

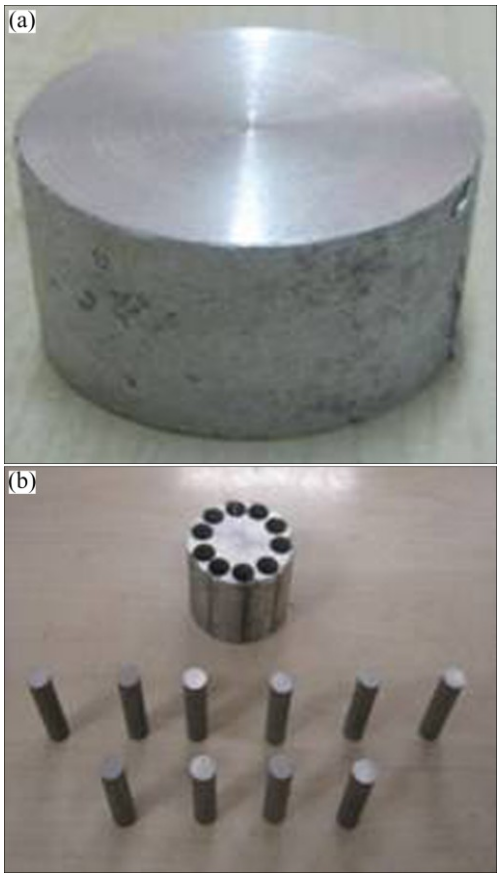

Fig. 3 Sequence of steps followed to make wear test specimen using EDM

Table 4 Wear test parameters

Parameter	Level 1	Level 2	Level 3
Load/N	20	30	40
Sliding distance/km	1	2	3

3 Results and discussion

3.1 Micro Vickers hardness

The micro Vickers hardness for the cast samples was found using Chroma Micro Vickers hardness tester. Three readings were taken at the applied load of 500 g for 15 s and the average hardness for Al−Gr was HV 74.6, for Al−Si_3N_4 nanocomposite, it was HV 78.5 and for Al−Gr−Si_3N_4 hybrid composite, it was HV 91.3. From the hardness, it was inferred that the bonding strength of hybrid composite increased, which may be due to additional presence of graphite, whereas the nanocomposite did not show much increase in hardness.

The cumulative sizes of graphite and Si_3N_4 nanoparticles were studied using SEM and are shown in Figs. 4 and 5, respectively. The size of the particles was confirmed from the test and found to be in the range of 500−600 nm; EDS showed the uniform distribution of Si_3N_4 particles in Al matrix composite. EDS analysis in Figs. 6 and 7 shows the presence of graphite in the form of carbon silicon nitride compound formed with other elements present.

3.2 Tensile strength analysis of hybrid composite

To analyze the mechanical properties of the sample, specimens were prepared to perform tensile test as per ASTM B557. The test was carried out in universal testing machine at the strain rate of 5 mm/min and machine has a maximum load carrying capacity of 100 t.

The typical stress and strain curves are shown in Fig. 8. The curves exhibit an initial elastic portion, a yield plateau (that is, a yield point beyond which the strain increases with increase in stress), a strain hardening range in which stress again increases with the increase of the strain, and finally a range in which the

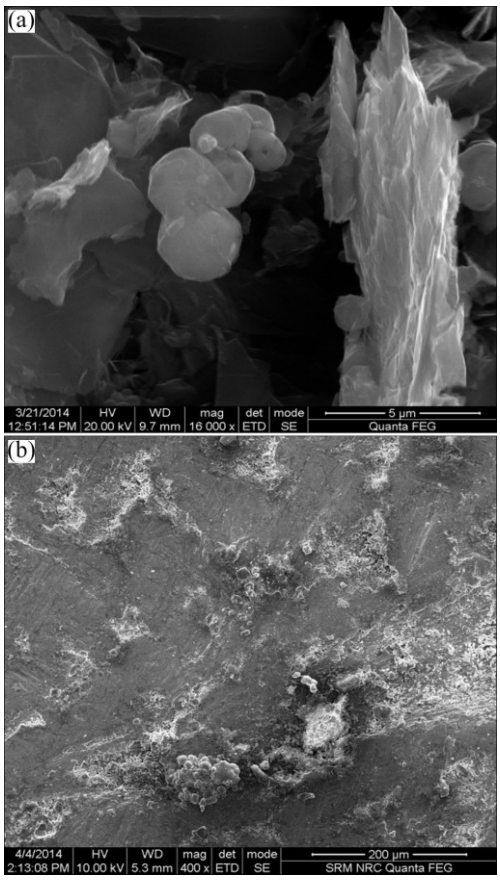

Fig. 4 SEM images of Gr powder (a) and Al−Gr (b) distribution

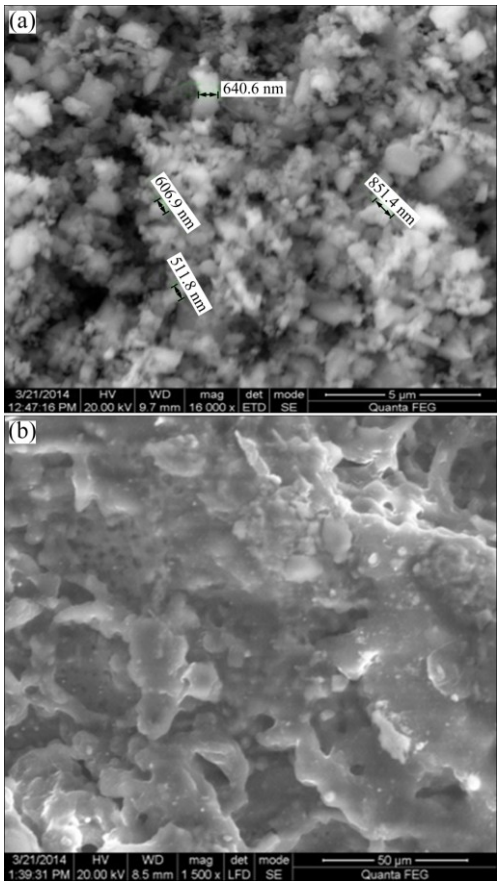

Fig. 5 SEM images of Si_3N_4 (a) and Al−Si_3N_4 (b) distribution in nanocomposite

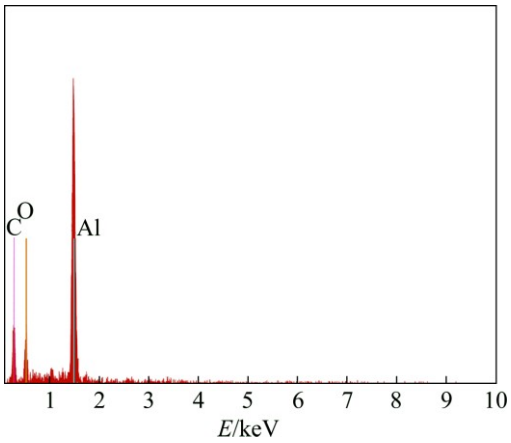

Fig. 6 EDS spectrum showing presence of graphite

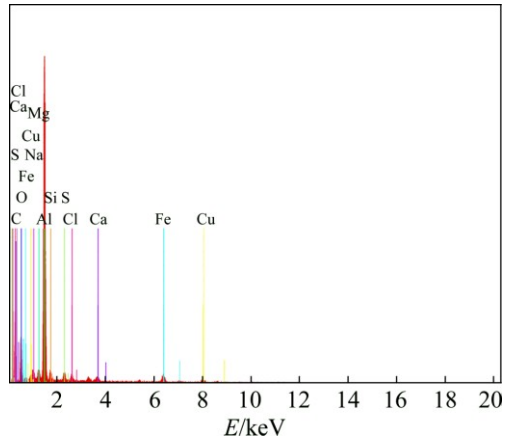

Fig. 7 EDS spectrum showing presence of Al, Gr and Si_3N_4

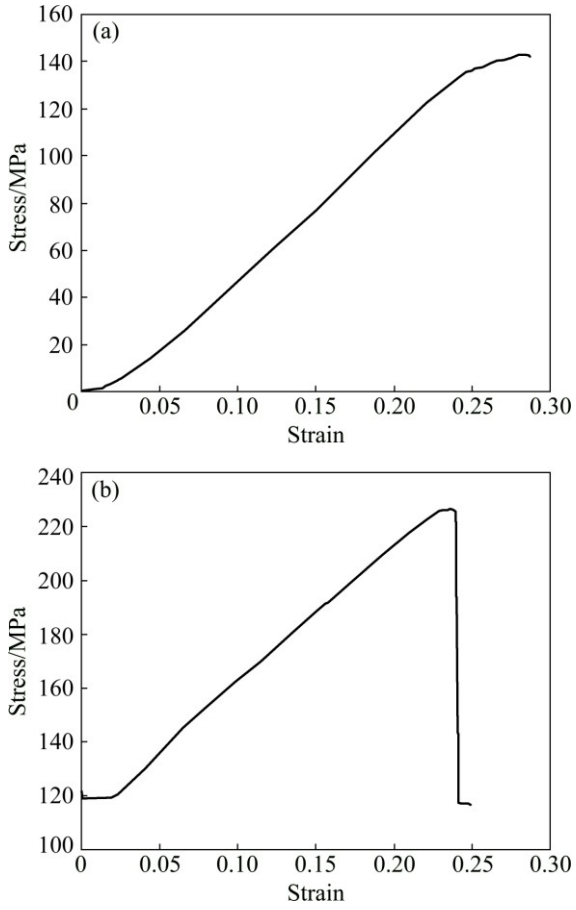

Fig. 8 Tensile strength for Al−Si_3N_4 composite (a) and Al−Gr−Si_3N_4 hybrid composite (b)

stress drops off until fracture occurs. The slope of the linear elastic portion of the curve represents the elastic modulus of hybrid composite. The stress at the yield point, referred as the yield strength, is a very important property of hybrid composite reinforcement. Reinforcement is generally characterized by its yield strength. The result of the tensile test shows that the hybrid composite has the strength of 226.3 MPa when compared with Al−Si_3N_4 composite of 142.8 MPa. The results show that tensile strength of the hybrid composite is 37% stronger than ordinary composite.

3.3 Wear behavior of Al−Si_3N_4 micro and nanocomposite

Sliding wear evaluation for the fabricated nanocomposite was carried out using pin-on-disc equipment as per ASTM G99 standards. For various loading and sliding distance conditions, the mass loss, volume loss, wear rate and coefficient of friction were determined for the test specimen. The experiments were conducted based on L9 orthogonal array. The coefficient of friction was calculated by taking the frictional force from Winducom. The effects of wear rate and coefficient of friction of Al−Gr, Al−Si_3N_4 and Al−Gr−Si_3N_4 components were analyzed and are listed in Table 5. The wear rate decreased as sliding distance increased. The volume loss of the material (V_a) could also be found using Archard's law of wear [15]. In this investigation, the mass loss procedure was used.

$$V_a=(a_b Nd)/H_b \quad (1)$$

where a_b is the wear coefficient of the Al−Si_3N_4 material, N is the applied normal load, d is the sliding distance in km and H_b is the hardness of the nanocomposite material.

Figure 9 confirms that with the increase in normal load, there was a decrease in coefficient of friction and it was observed for both Al−Si_3N_4 micro and Al−Si_3N_4 nanocomposites.

3.4 Effect of normal load on mass loss

From Fig. 10, it is observed that with an increase in normal load, an increase in mass loss was also observed in case of both Al−Gr and Al−Si_3N_4 nanocomposite, whereas for Al−Gr−Si_3N_4 hybrid composite there was slight decrease in mass loss for 30 N load and then there was an increase in mass loss. The reason for less mass loss was that at lower loads the contact plateaus were less and hence there was reduced wear for both the Al−Gr and Al−Si_3N_4 nanocomposites whereas for the Al−Si_3N_4 nanocomposite at higher loads, the contact plateaus were more and hence mass loss also increased. There was greater variation in the mass loss of Al−Si_3N_4 nanocomposite for the sliding distance of 3 km at 40 N which may be due to more dislodgement of particles. The micro hardness for the nanocomposite was less by 14% which ensured that dislodged particle acted as abrasive particle. The mass loss was observed to be less in case of Al−Gr−Si_3N_4 hybrid nanocomposite than nanocomposite as the graphite acted as solid lubricant, and hence there was less dislodgement of Si_3N_4 from Al matrix.

Table 5 Wear rate and coefficient of friction details for Al−Gr, Al−Si_3N_4 nanocomposite and Al−Gr−Si_3N_4 hybrid composite

Sliding distance/km	Load/N	Al−Gr			Al−Si_3N_4			Al−Gr−Si_3N_4		
		Volume loss/mm^3	Wear rate/($mm^3 \cdot km^{-1}$)	COF	Volume loss/mm^3	Wear rate/($mm^3 \cdot km^{-1}$)	COF	Volume loss/mm^3	Wear rate/($mm^3 \cdot km^{-1}$)	COF
1	20	0.0379	0.0378	0.49	0.2487	0.248	0.295	0.1754	0.1754	0.25
2	30	0.0822	0.0411	0.32	5.8536	2.926	0.438	1.8070	0.9035	0.36
3	40	0.1520	0.0505	0.23	16.2845	5.428	0.495	9.7192	3.2397	0.43
1	30	0.0380	0.0382	0.47	0.2845	0.284	0.386	0.217	0.2176	0.36
2	40	0.0909	0.0454	0.24	7.1788	3.589	0.452	5.5614	2.7807	0.40
3	20	0.1140	0.0380	0.36	7.8780	2.626	0.43	2.9298	0.9766	0.28
1	40	0.0568	0.0568	0.45	0.4837	0.483	0.465	0.3807	0.3807	0.38
2	20	0.0766	0.0382	0.38	4.2520	2.126	0.395	1.4561	0.7280	0.25
3	30	0.1290	0.0429	0.27	8.9268	2.975	0.476	2.1228	0.7076	0.40

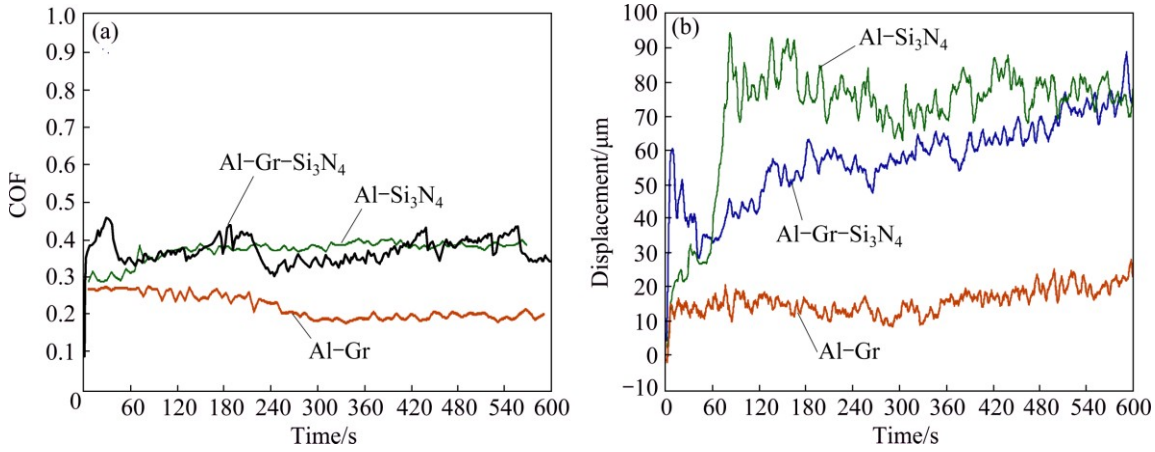

Fig. 9 Comparison of wear behavior of all three composites: (a) Coefficient of friction−time curve; (b) Displacement−time curve for Al−Gr−Si_3N_4 hybrid composite

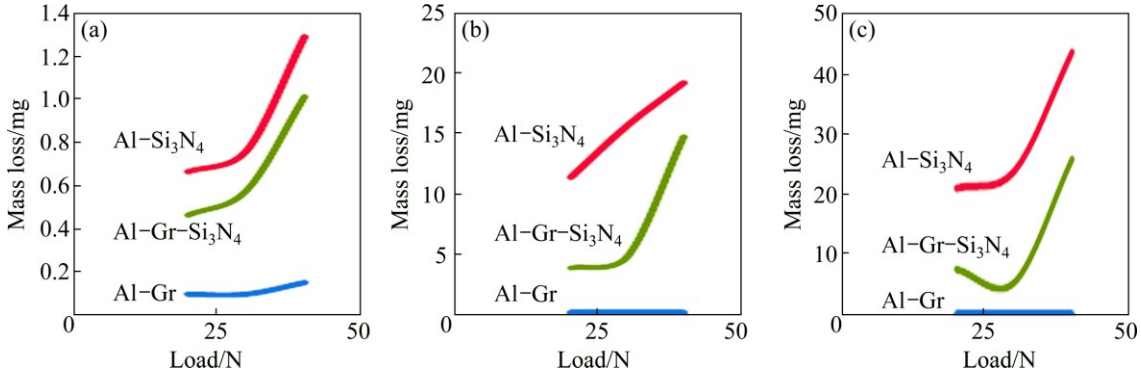

Fig. 10 Comparison of normal load vs mass loss for sliding distances of 1 km (a), 2 kms (b) and 3 km (c)

3.5 Effect of normal load on wear rate

From Fig. 11, it is observed that with an increase in normal load, an increase in wear rate was observed for Al−Gr, Al−Si_3N_4 nanocomposite and Al−Gr−Si_3N_4 hybrid composite, the reason for increase in wear rate with normal load was that at lower load the contact area was less and hence reduced wear for both the Al−Si_3N_4 nano and Al−Gr−Si_3N_4 hybrid nanocomposites while at higher loads, the contact plateaus were also more, hence causing the increased wear [8]. At higher loads the composite material was forced against the disc, thereby increasing the wear rate. The wear rate was observed to be less in case of Al−Gr, as graphite acted as solid lubricant, leading to tribo layer formation, whereas for nano and hybrid composites the Si_3N_4 reinforcement could dislodge and would act as abrasive, leading to three-body abrasive mechanism and hence more wear was likely to be observed. But the wear rate for the hybrid composite was less, which may be due to presence of graphite and the same could be inferred from

the increase of hardness.

3.6 Effect of normal load on coefficient of friction

It is observed from Fig. 12 that, with the increase in normal load, there was a decrease in coefficient of friction for Al−Gr composite whereas for hybrid and nanocomposite, there was a gradual initial increase and then it would stabilize. This may be due to formation of tribolayer on the contact surface as there would be transfer of material from either the pin or disc material to each other during sliding, i.e., adhesion mechanism on the surface will take place. During initial rubbing, the film (tribolayer) breaks up and clean surfaces come in contact. For a higher load, the rate of formation of tribolayer will be higher as the temperature rises in the contact area due to which plastic deformation on the surface will take place; hence, it was observed that there was a decrease in coefficient of friction as load increased. On continuous sliding there will be formation of microcracks which propagates and over a period of time its surface breaks up. This in turn enhances the braking system of the vehicle.

3.7 SEM analysis

In order to assess the wear behavior, the worn surface was analyzed using SEM and the surface topography of the hybrid and nanocomposites for 100 μm was captured. The wear behavior of the hybrid and nanocomposites was analyzed for sliding distance of 2 km subjected to normal load of 40 N and for sliding distance of 3 km subjected to normal load of 40 N. The same loading conditions were chosen so that the comparison could be made. From Fig. 13, it could be observed that the hybrid composite showed less

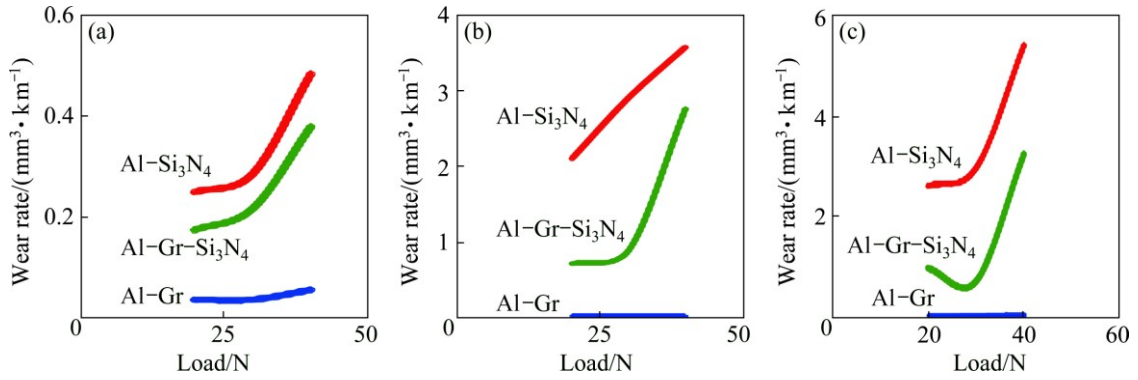

Fig. 11 Comparison of wear rates for different sliding distances of 1 km (a), 2 km (b) and 3 km (c)

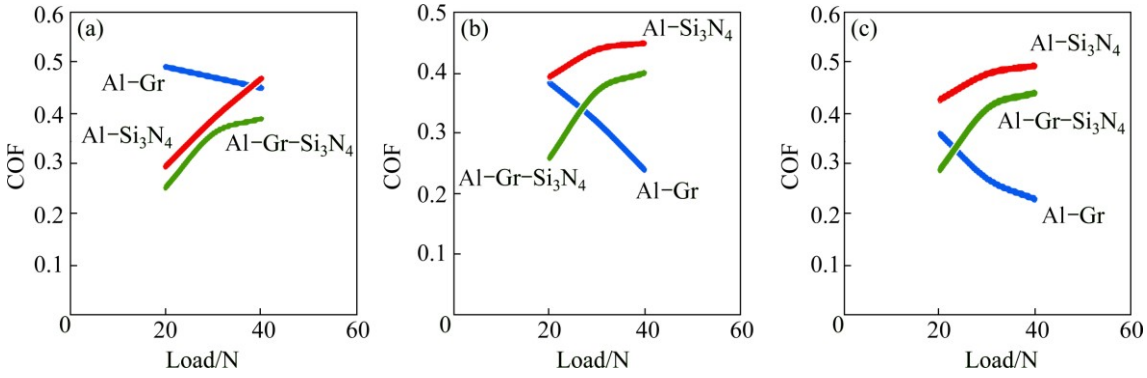

Fig. 12 Comparison of COF for different sliding distances of 1 km (a), 2 km (b) and 3 km (c)

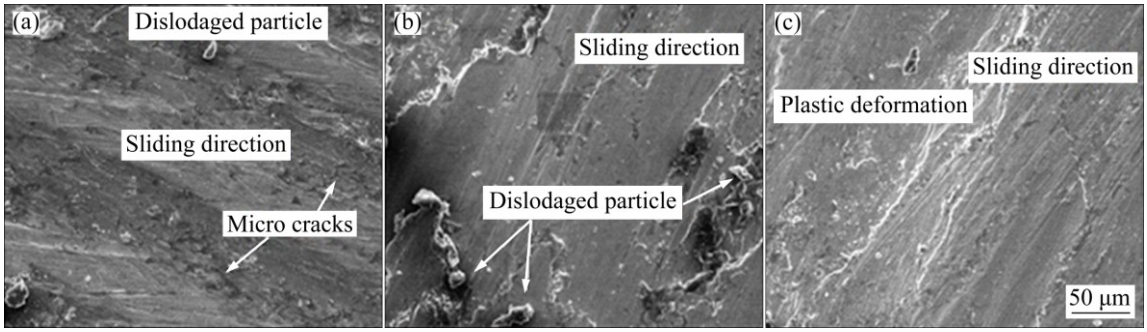

Fig. 13 SEM images of wear analysis of 100 μm Al−Si_3N_4 nanocomposite (a), Al−Gr−Si_3N_4 hybrid composite (b) and Al−Gr composite (c)

microcracks or pits and the tribolayer formation was uniform; whereas in the nanocomposite there were lots of pits, dislodgement of particles and no uniform tribolayer formation leading to higher wear rate and COF. Adhesion of the worn particles was also observed for hybrid composite along the sliding direction. This adhesion itself would act as an abrasive material, leading to wear, resulting in an increase in wear rate. It was evident that the worn surface of Al−Gr composite had fairly more uniform plastic deformation, leading to tribolayer formation, in turn leading to more uniform wear rate.

3.8 Surface plots to compare wear rate of hybrid and nanocomposite

3D surface plots were generated as shown in Fig. 14

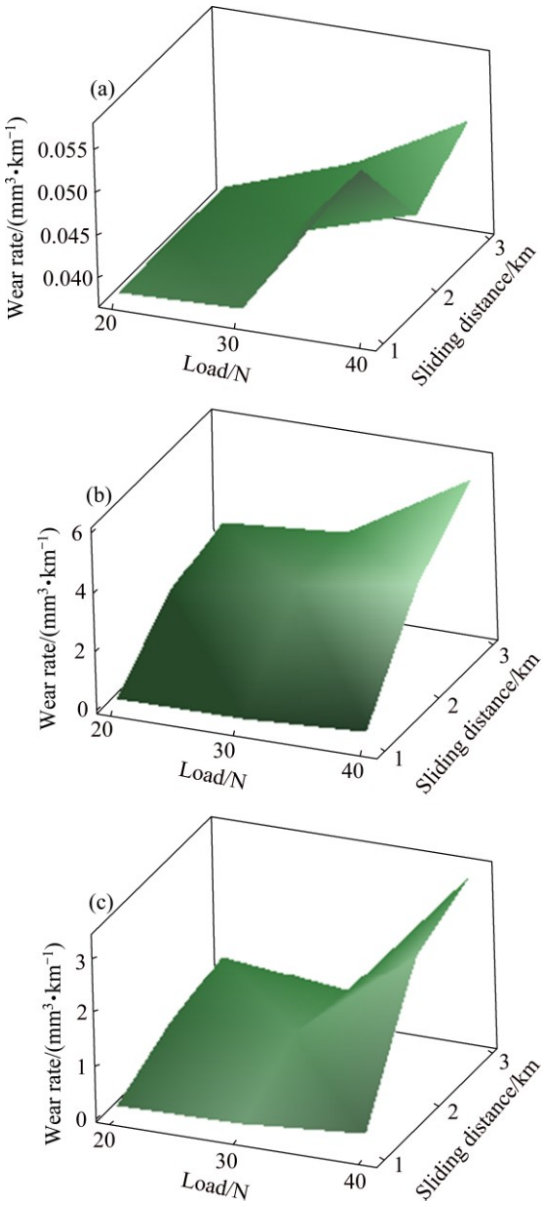

Fig. 14 3D surface plots of wear rate of Al−Gr (a), Al−Si_3N_4 (b) and Al−Gr−Si_3N_4 hybrid composite (c)

for Al−Gr, Al−Si_3N_4 and Al−Gr−Si_3N_4 individually to find the effect of the sliding distance and load against the response variable wear rate. It was inferred from the 3D graph that as the sliding distance and load increased the wear rate decreased. Initially, when the surface was in contact at lower loads the contact area was less and hence few points would be in contact with the disk material, leading to more wear as full load would be acting on these contact points.

As the sliding distance increased for all the loads, wear rate was less, this was due to the fact that the formation of tribolayer was more. When the sliding distance increased due to the fact that the temperature at contact increased, adhesion of pin material to disk took place, leading to more tribolayer formation. At sliding distance of 2 km, the wear rate was more for hybrid and nanocomposite and then it stabilized. The wear of hybrid composite was less when compared with nanocomposite because the presence of graphite in the hybrid composite acted as solid lubricant, causing less wear. More wear was observed for Al−Si_3N_4 when compared with the hybrid composite. The wear rate of Al−Gr composite was less when compared with Al−Si_3N_4 and Al−Gr−Si_3N_4 hybrid composite. More darker regions were obtained for Al−Si_3N_4 nanocomposite as the dislodgement of the material was more and the dislodged materials acted as abrasive, leading to more wear. The presence of Gr in the hybrid composite acted as a solid lubricant, leading to formation of tribolayer reducing the wear rate.

3D surface plots were generated as shown in Fig. 15 for Al−Gr, Al−Si_3N_4 and Al−Gr−Si_3N_4 individually to find the effect of the sliding distance and load against the response variable coefficient of friction. It can be inferred from the 3D graph that as the sliding distance and load increased, the coefficient of friction increased. Initially, when the surface was in contact at lower loads, the contact area was less and hence fewer points were in contact, thereby causing minimal friction. As the sliding distance and load increased, the coefficient of friction was more, this was due to the fact that the formation of tribolayer gradually increased and then it stabilized. The Si_3N_4 will act as abrasive material, leading to more wear in the tribolayer formed with exposed fresh layer coming into contact. The COF of hybrid composite was less when compared with nanocomposite because the presence of graphite in the hybrid composite acted as solid lubricant causing more tribolayer formation. For Al−Gr composite, there was gradual decrease in COF. The graphite present in the composite acted as lubricant, promoting the tribolayer formation.

3.9 ANOVA analysis

Analysis of variance (ANOVA) test was performed to identify the most effective process load parameters

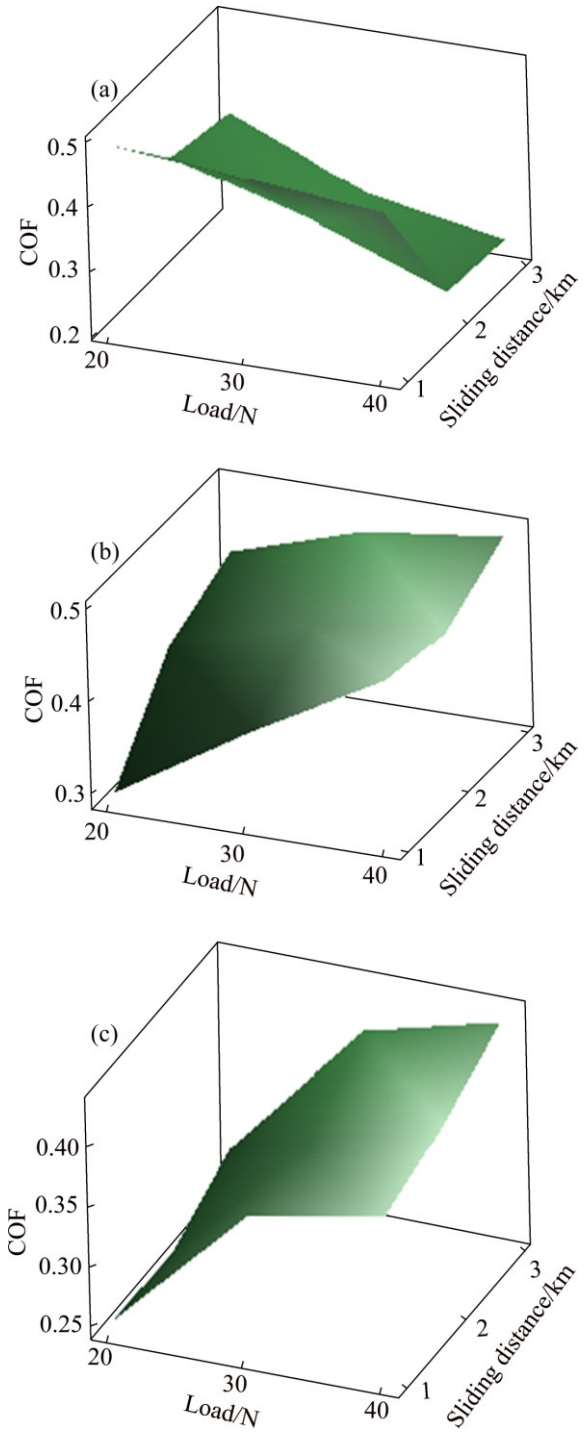

Fig. 15 3D surface plots of coefficient of friction for Al−Gr (a), Al−Si_3N_4 (b) and Al−Gr−Si_3N_4 hybrid composite (c)

which affect the wear rate of Al−Gr composite as shown in Tables 6−8 for different composites. The results of ANOVA indicated that sliding distance parameters had significant contribution to the wear rate of Al−Gr−Si_3N_4 hybrid composite materials with a percentage contribution of 45.63%, followed by load of 43.39%. Similarly, according to the analysis of variance results, the sliding distance of Al−Si_3N_4 composite had 75.98% contribution followed by load with 15.10% contribution. Thus, the most effective wear factor on the hybrid composite was sliding distance on the material (*R-Sq*= 89.93%). Based on *P*-value, the relative importance of the factor effect on relative closeness coefficient could be identified for hybrid composites. As the *P* value decreased, the contribution increased. When the *P* value was less than 0.5, it denoted that the sliding distance parameter of hybrid composite was more significant in determining the wear characteristics of the material.

4 Conclusions

1) The mass loss increased as the normal load increased for all Al−Gr, Al−Si_3N_4 nanocomposite and Al−Gr−Si_3N_4 hybrid composites. Al−Si_3N_4 nanocomposite exhibited more mass loss when compared with Al−Gr−Si_3N_4 hybrid composite for all sliding distances. This was due to the factor of less dislodgement of material from the surface of hybrid composite and the same could be confirmed from nicro Vicker hardness test. The presence of graphite in the matrix had good influence on the bonding strength and hence higher hardness value was achieved for the hybrid composite.

2) There was 25% decrease in wear rate for Al−Gr−Si_3N_4 hybrid composites when compared with Al−Si_3N_4 nanocomposite for the sliding distance of 1 km. The wear rate of Al−Gr−Si_3N_4 hybrid composite was found to decrease by 65% for the loads of 20 and 30 N. The presence of graphite in the hybrid matrix acted as solid a good lubricant leading to more tribolayer formation and lesser wear. The wear rate of Al−Gr was very minimal and the micro Vicker hardness was also less. From the obtained results it was inferred that it may not be a suitable substitute for braking application.

Table 6 ANOVA for wear rate of Al−Gr composite

Machining parameter	Degree of freedom, f	Sum of squares, SS_A	Variance/V_A	F_{ao}	P	Contribution/%
Sliding distance/km	2	0.000012	0.000006	0.39	0.700	3.38
Load/N	2	0.000277	0.000139	8.66	0.035*	78.15
Error	4	0.000064	0.000032			18.47
Total	8	0.000354				100

*Significant; *R-Sq*=81.90%; *R-Sq* (adj)=63.79%

Table 7 ANOVA for wear rate for Al−Si_3N_4 composite

Machining parameter	Degree of freedom, f	Sum of squares, SS_A	Variance/V_A	F_{ao}	P	Contribution/%
Sliding distance/km	2	18.238	9.1188	17.03	0.011*	75.98
Load/N	2	3.627	1.8135	3.39	0.138	15.10
Error	4	2.142	0.5354			8.92
Total	8	24.006				100

*Significant; *R-Sq*=91.08%; *R-Sq* (adj)=82.16%

Table 8 ANOVA for wear rate for Al−Gr−Si_3N_4 Hybrid composite

Machining parameter	Degree of freedom, f	Sum of squares, SS_A	Variance/V_A	F_{ao}	P	Contribution/%
Sliding distance/km	2	4.514	2.257	4.87	0.085*	45.63
Load/N	2	4.294	2.147	3.62	0.127	43.39
Error	4	1.087	0.543			10.98
Total	8	9.895				100

*Significant; *R-Sq*=89.93%; *R-Sq* (adj)=71.86%

3) Al−Gr−Si_3N_4 hybrid composite exhibited around 15% reduction in coefficient of friction when compared with Al−Si_3N_4 nanocomposite, leading to less wear, this was due to less dislodgement of materials from bulk when compared with the nanocomposite. The worn particle adhered to the surface, leading to severe wear on the tribo-film. The same could be seen in the SEM images for nanocomposite. But there was uniform tribolayer formation in hybrid and graphite composites as the graphite acts as solid lubrication.

4) The results of ANOVA indicated that sliding distance parameters had significant contribution to the wear rate of Al−Gr−Si_3N_4 hybrid composite materials with a percentage contribution of 45.63% for sliding distance, followed by load of 43.39% contribution. Similarly, according to the analysis of variance results, for the Al−Si_3N_4 composite, sliding distance had 75.98% contribution followed by load with 15.10% contribution.

References

[1] KAUSHIK N C, RAO R N. The effect of wear parameters and heat treatment on two body abrasive wear of Al−SiC−Gr hybrid composites [J]. Tribology International, 2016, 96: 184−190.

[2] SAEED B, MOHAMMAD T, EHSAN B. Fabrication and characteristic of Al-based hybrid nanocomposite reinforced with WO_3 and SiC by accumulative roll bonding process [J]. Journal of Alloys and Compounds, 2015, 653: 39−46.

[3] KENNETH K A, TOLULOPE M A, PETER A O. Corrosion and wear behavior of Al−Mg−Si alloy matrix hybrid composites reinforced with rice husk ash and silicon carbide [J]. Materials Technology, 2014, 3: 9−16.

[4] SARADA B N, SRINIVASA M P L, UGRASEN G. Hardness and wear characteristics of hybrid aluminium metal matrix composites produced by stir casting technique [J]. Materials Today, 2015, 2(4−5): 2878−2885.

[5] POZDNIAKOV A V, ZOLOTOREVSKIY V S, BARKOV R Y, LOTFY A, BAZLOV A I. Microstructure and material characterization of 6063/B_4C and 1545K/B_4C composites produced by two stir casting techniques for nuclear applications [J]. Journal of Alloys and Compounds, 2016, 664: 317−320.

[6] BALAJI V, SATEESH N, MANZOOR H M. Manufacture of aluminium metal matrix composite (Al7075−SiC) by stir casting technique [J]. Materials Today: Proceedings, 2015, 2(4−5): 3403−3408.

[7] HAMID R E, SEYED A S, MOHSEN H S, HUANG Y Z. Investigation of microstructure and mechanical properties of Al6061-nanocomposite fabricated by stir casting [J]. Materials and Design, 2014, 55: 921−928.

[8] YIN Zeng-bin, YUAN Jun-tang, HUANG Chuan-zhen, WANG Zhen-hua, HUANG Lei, CHENG Yu. Friction and wear behaviors of Al_2O_3/TiC micro-nano-composite ceramic sliding against metals and hard materials [J]. Ceramics International: Part B, 2016, 42(1): 1982−1989.

[9] PARDEEP S, SATPAL S, DINESH K. Production and some properties of Si_3N_4 reinforced aluminium alloy composites [J]. Journal of Asian Ceramic Societies, 2015, 3: 352−359.

[10] XIU Zi-yang, CHEN Guo-qin, WU Gao-hui, YANG Wen-shu, LIU Yan-mei. Effect of volume fraction on microstructure and mechanical properties of Si_3N_4/Al composites [J]. Transactions of Nonferrous Metals Society of China, 2011, 21: 285−289.

[11] MATHAN K, SENTHIL K, KUMARA S L A. High temperature investigation on EDM process of Al 2618 alloy reinforced with Si_3N_4, ALN and ZrB_2 in-situ composites [J]. Journal of Alloys and Compounds, 2016, 663: 755−768.

[12] WANG Shi-long, HUANG Xue-fei, GONG Meng-xiao, HUANG Wei-gang. Microstructure and mechanical properties of Ni−P−Si_3N_4 nanowire electroless composite coatings [J]. Applied Surface Science Part A, 2015, 357: 328−332.

[13] HUANG Yu, LIN Jia, ZHANG Hou-an. Effect of Si_3N_4 content on microstructures and antioxidant properties of $MoSi_2$/Si_3N_4 composite coatings on Mo substrate [J]. Ceramics International, 2015, 41: 13903−13907.

[14] TOMASZ C, JAROSLAW W, MAREK K, BOGUSLAWA A C, ANDRZEJ O. Influence of graphene addition and sintering temperature on physical properties of Si_3N_4 matrix composites [J]. International Journal of Refractory Metals and Hard Materials, 2016, 57: 19−23.

[15] JAN B, PAVOL H, JAN D, CSABA B, JANA G. Wear damage of Si_3N_4−graphene nanocomposites at room and elevated temperatures [J]. Journal of the European Ceramic Society, 2014, 34(14): 3309−3317.

[16] BARADESWARAN A, VETTIVEL S C, ELAYA P A, SELVAKUMAR N, FRANKLIN I R. Experimental investigation on mechanical behaviour, modelling and optimization of wear parameters of B_4C and graphite reinforced aluminium hybrid composites [J]. Materials and Design, 2014, 63: 620−632.

干滑动摩擦条件下 Al−Si_3N 纳米复合材料及 Al−Gr−Si_3N_4 混杂复合材料摩擦磨损性能的优化

R. AMBIGAI, S. PRABHU

Department of Mechanical Engineering, SRM University, Chennai 603203, India

摘　要：研究含石墨(Gr)和氮化硅纳米颗粒金属型搅拌铸造 LM16 合金的摩擦学性能。在干滑动摩擦条件下分别制备 Al−Gr−Si_3N_4 混杂复合材料、Al−Si_3N_4 和 Al−Gr 纳米复合材料。采用 EDS 测试技术确保 Si_3N_4 纳米颗粒和石墨在铸件中的均匀分布。采用 L9 正交实验方法进行实验以研究应用载荷(20, 30 和 40 N)和滑动距离(1, 2 和 3 km)对合金摩擦磨损性能的影响。结果表明：与 Al−Si_3N_4 纳米复合材料相比，Al−Gr−Si_3N_4 混杂复合材料的磨损率和摩擦因数(COF)分别降低了 25%和 15%，而 Al−Gr 纳米复合材料的磨损率和 COF 很小。混杂复合材料的显微维氏硬度比普通复合材料的提高了 14%，而 Al−Gr 和 Al−Si_3N_4 纳米复合材料的显微硬度无明显变化。用扫描电镜对合金磨损表面和次表面的组织进行观察。结果表明，纳米复合材料的主要磨损机理为磨粒磨损，而混杂复合材料的主要磨损机理为磨粒磨损和粘着磨损。方差分析(AVOVA)和 *F* 检验用于验证模型的有效性及确定影响磨损率的显著性参数。

关键词：磨粒磨损；Si_3N_4；石墨；混杂复合材料；载荷；滑动距离；方差分析

(Edited by Wei-ping CHEN)